SOILS AND FOUNDATIONS Vol. 31, No. 2, 93-107 June 1991
Japanese Society of Soil Mechanics and Foundation Engineering

ELASTO-VISCOPLASTIC CONSOLIDATION OF A DIATOMACEOUS MUDSTONE

HARUYOSHI MAEKAWA[i], KEI MIYAKITA[ii]
and HIDEO SEKIGUCHI[iii]

ABSTRACT

This paper discusses the consolidation behaviour of a diatomaceous mudstone, which is best featured as a naturally cemented material having a highly porous skeleton. Part I of the paper presents the results of isotropic consolidation tests as well as falling-head permeability tests, all of which were performed on undisturbed specimens of the mudstone by using a high-pressure triaxial cell. The principal findings include: (1) the mudstone exhibits distinct yielding when it straddles the pre-consolidation pressure; (2) the secondary compression is negligibly small before the initial yielding, but becomes very pronounced when loaded sensibly above the pre-consolidation pressure; and (3) the logarithm of the coefficient of permeability decreases linearly with decreasing void ratio.

In part II of the paper, an associated series of coupled-stress flow analyses of the consolidation tests is performed in terms of the method of finite elements. An adapted version of the elasto-viscoplastic constitutive model (Sekiguchi, 1977) is implemented into the analysis procedure. The procedure of determining the constitutive parameters is described. It is then shown that the predicted performances compare favourably with the measured performances of consolidation in a consistent manner, thus validating the relevance of the elasto-viscoplastic formulation adopted.

Key words: consolidation test, constitutive equation of soil, finite element method, mudstone, permeability, plasticity, rheology, secondary compression, water pressure, yield (**IGC**:D5/E2)

INTRODUCTION

Thick deposits of diatomaceous mudstones of Tertiary period are distributed in the Noto Peninsula, Japan (see Fig. 1). Some of them have been mined to give raw materials for engineering products such as fire-resistant bricks, portable furnaces and so forth, by taking advantage of the fact that the mudstones contain a lot of silica-rich, porous diatoms in

[i] Lecturer, Department of Civil Engineering, Kanazawa Institute of Technology, 7-1, Ohgigaoka, Nonoichi-machi, Ishikawa-gun, Ishikawa 921.
[ii] Professor, ditto.
[iii] Associate Professor, Disaster Prevention Reseach Institute, Kyoto University, Gokasho, Uji, Kyoto 611.
Manuscript was received for review on February 2, 1990.
Written discussion on this paper should be submitted before January 1, 1992, to the Japanese Society of Soil Mechanics and Foundation Engineering, Sugayama, Bldg. 4 F, Kanda Awaji-cho 2-23, Chiyoda-ku, Tokyo 101, Japan. Upon request the closing date may be extended one month.

their skeleton.

Geotechnical properties of those mudstones have recently received much attention. The construction of a 1050-meter long, pile-supported bridge over Nanao Bay underlain by the Wakura diatomaceous mudstone was epochmaking in this regard (Yamada and Matsuse, 1981; Nishida et al., 1985). Indeed it has not only aroused a specific interest in the performance of steel pipe piles driven into that mudstone, but has helped to call for an integrated knowledge about the basic, mechanical properties of those diatomaceous mudstones in general (Maekawa and Miyakita, 1983; Sekiguchi et al., 1985 among others).

The present paper consists of two parts. Part I will present an organized set of data of the isotropic consolidation tests on undisturbed specimens of a diatomaceous mudstone sampled from Suzu. An emphasis will be placed on the consolidation behaviour when straddling the pre-consolidation pressure, p_c'. Note that the terminology "pre-consolidation pressure" is used hereinafter to refer specifically to the inviscid initial-yield pressure such as illustreted in Fig. 2. The permeability characteristics of the mudstone will be quantified directly from falling-head permeability tests. In Part II of the paper, those sets of experimental data will be utilized as a sort of "data base", against which the predictive capability of an elasto-viscoplastic constitutive model (Sekiguchi, 1977) will be assessed, along with coupled stress-flow analyses of the consolidation tests in terms of the method of finite elements.

PART I
EXPERIMENTAL INVESTIGATION

THE DIATOMACEOUS MUDSTONE INVESTIGATED

The diatomaceous mudstone studied in this paper was sampled in the form of undisturbed blocks, 400 mm in each direction, from the face of an adit of a furnace factory in Suzu city (Fig. 1). The mudstone was remarkably homogeneous, intact and fully saturated in the field. Its basic, physical properties are summarized in Table 1. The very porous nature of the mudstone can be noticed from the high value of natural void ratio, e_n, and the low specific gravity, G_s. The value of pre-consolidation pressure $p_c'=25$ kgf/cm^2 (2.45 MPa) could then be said "very high", in view of such a porous skeleton of the mudstone, suggesting the occurrence of distinct breakdown in structure when loaded beyond p_c'. This will prove to be the case later in this paper.

Table 1. Physical properties of the diatomaceous mudstone from Suzu, Noto Peninsula

Natural water content:	w_n =116.7%
Natural void ratio:	e_n =2.576
Specific gravity:	G_s =2.233
Unit density:	ρ_t =1.353 g/cm^3
Unconfined compressive strength:	q_u =20.7 kgf/cm^2 (2.03 MPa)
Pre-consolidation pressure:	p_c' =25 kgf/cm^2 (2.45 MPa)

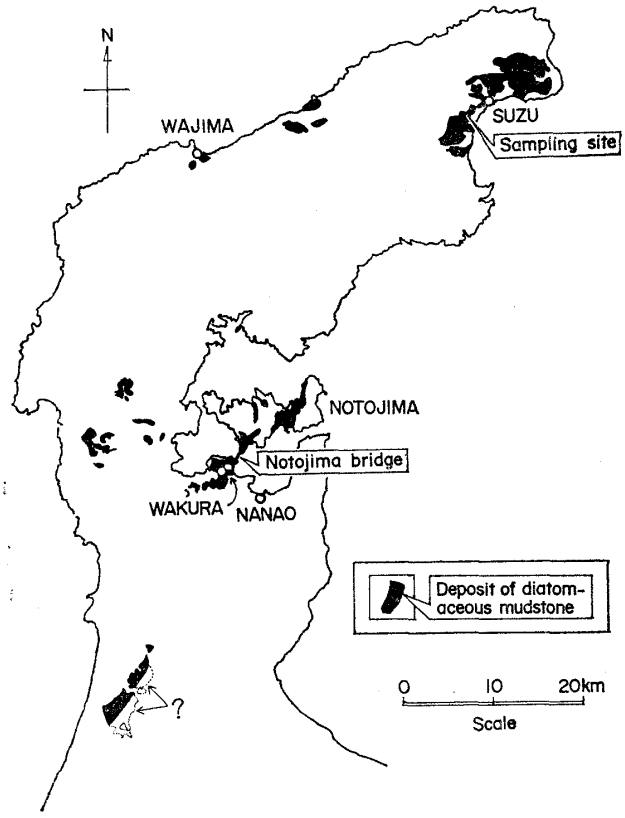

Fig. 1. Distribution of diatomaceous mudstones in the Noto Peninsula, Japan

EXPERIMENTAL PROCEDURE

The present experimental program consists of isotropic consolidation tests and falling-head permeability tests. All the tests were performed on cylindrical specimens of 50 mm in diameter and 100 mm long, by using a triaxial cell having a maximum, allowable pressure of 75 kgf/cm² (7.35 MPa). Drainage in the consolidation tests was allowed only from the top surface of the specimen, and the porewater pressures at the base of the specimen were measured with an electric transducer of strain-gauge type.

Isotropic Consolidation Tests

A total of five isotropic consolidation tests was performed on five identical specimens of the mudstone, at different consolidation pressures. The loading conditions adopted are illustrated in Fig. 2. Each specimen was initially brought to equilibrium under a confining pressure p_o=0.5 kgf/cm² (0.049 MPa). Then it was subjected instantaneously to an increment of pressure to reach a prescribed confining pressure, p_f, and was left to consolidate with time at that pressure. The consolidation pressures selected were 20, 30, 40, 55 and 70 kgf/cm² (1.96, 2.94, 3.92, 5.39, 6.86 MPa). Note that all but one specimen straddled the pre-consolidation pressure, $p_c' = 25$ kgf/cm² (2.45 MPa) during their consolidation pressures.

Falling-Head Permeability Tests

Staged, falling-head permeability tests were performed on an undisturbed specimen of the mudstone so that the variation in permeability with void ratio may directly be assessed. The sequence of the permeability tests is illustrated in Fig. 3.

Each permeability test was designed to commence when the consolidation phase of the specimen at a given pressure had substantially been completed. This procedure proved to apply nicely to the first three tests in which the specimen remained essentially elastic. However, it was felt necessary to modify the procedure when the specimen underwent the

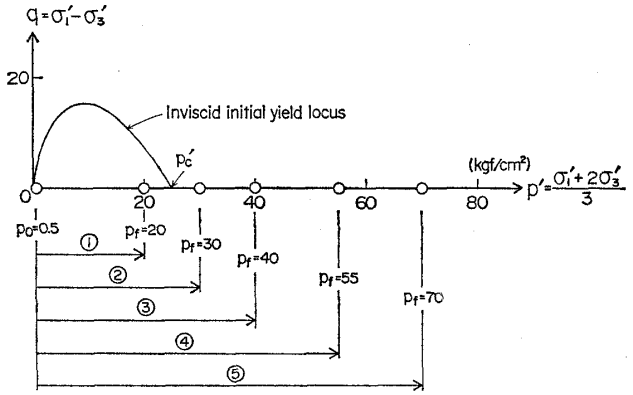

Fig. 2. Loading conditions for the isotropic consolidation tests

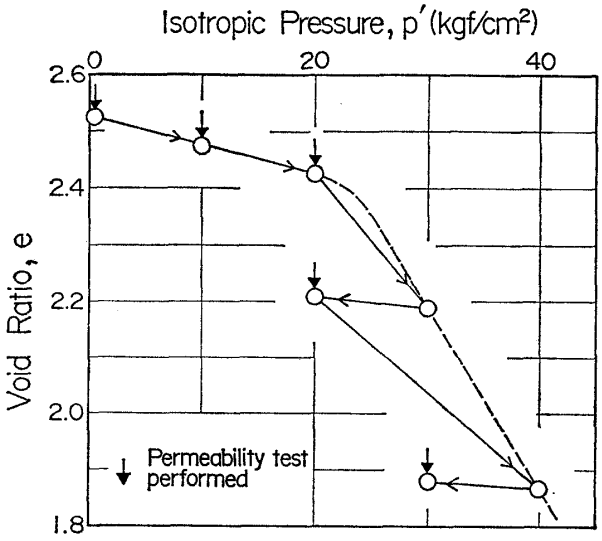

Fig. 3. Sequence of the falling-head permeability tests

initial yielding at $p=p_c'$ and started to exhibit marked creep under a constant effective stress. This is the reason why the specimen was allowed to rebound in the later two tests before going into the permeability testing.

In all the five permeability tests an initial excess head of 1.45 meters in water was carefully applied to the base of the specimen by means of a water-filled, graduated glass tube of 5 mm in diameter. The upward seepage in the specimen was thus allowed to occur in a steady-state fashion, and the associated drop in water level in the stand-pipe was measured for 24 hours. The drainage system connected to the specimen base was then closed, and the specimen was consolidated again at a higher

pressure to take a lower void ratio and the permeability testing was resumed as appropriate.

PRESENTATION OF EXPERIMENTAL RESULTS

Isotropic Consolidation Tests

Let $\bar{\varepsilon}_v$ be the overall volumetric strain of a specimen undergoing consolidation. That is,

$$\bar{\varepsilon}_v = (V_o - V) / V_o$$

where V and V_o respectively denote the current and the initial volume of the specimen.

The measured volume changes with time in all the five isotropic consolidation tests are shown in Fig. 4. Hereunder time $t = 0$ refers to the instant when the confining pressure, p, was increased to p_f. It is seen that the shape of the compression curve in test 2 differs markedly from more familiar shape such as observed in tests 3, 4, and 5. This well reflects the fact that in test 2 the ratio p_f/p_c' is as small as 1.2 and the influence of creep becomes relatively higher (Leonards and Girault, 1961).

The measured variations with time in the excess porewater pressure, p_w, at the base of each specimen, are shown in Fig. 5. It is seen that the excess porewater pressures in tests 1 and 2 dissipate almost completely within some

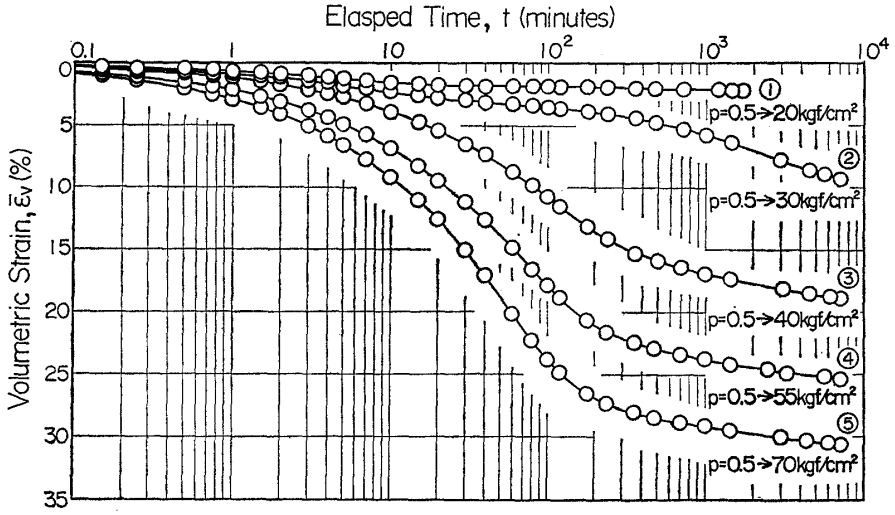

Fig. 4. Measured developments of the overall volumetric strain with time

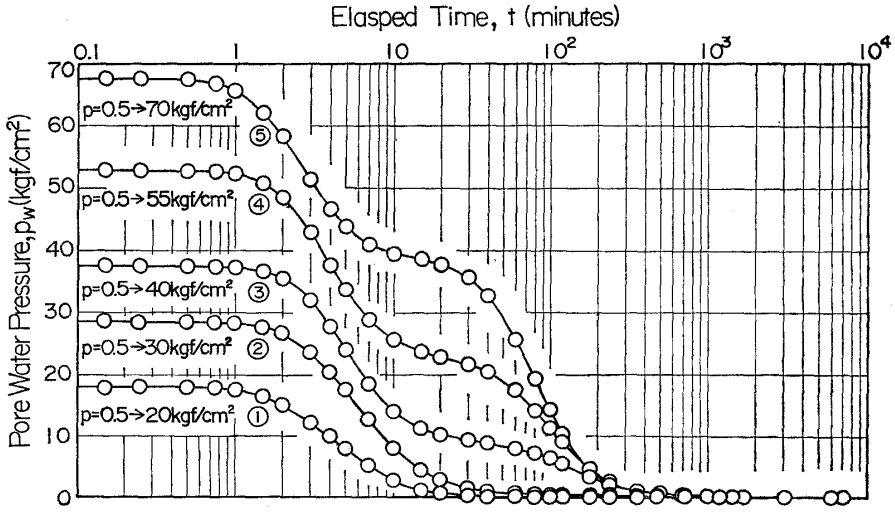

Fig. 5. Measured processes of dissipation of the excess porewater pressure at the specimen base with time

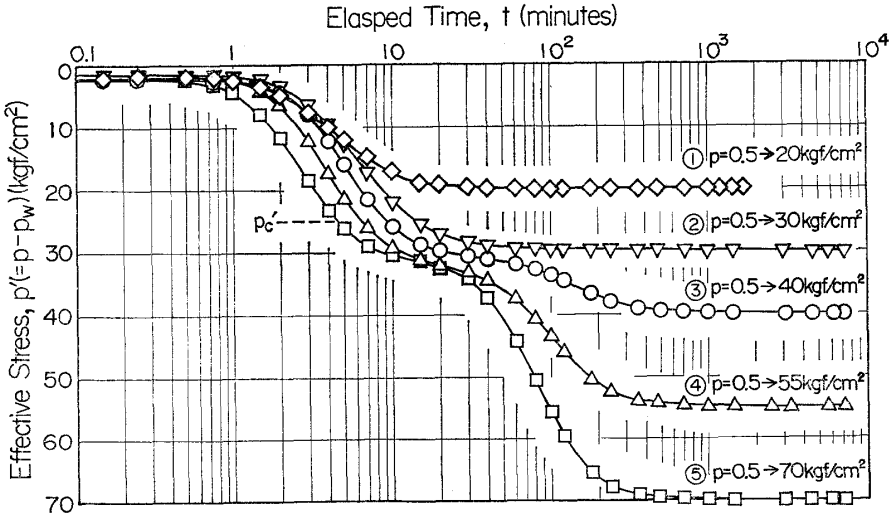

Fig. 6. Measured developments of the effective pressure at the specimen base with time

20 minutes. The pattern of behaviour different from this can be noticed for tests 3, 4 and 5. That is to say, the $p_w - \log t$ curve in each of those tests exhibits the "double sigmoid". The first sigmoidal portion until $t = 20$ minutes or thereabouts reflects the essentially elastic behaviour of the overconsolidated specimen before yielding. The second sigmoid reflects the inelastic behaviour of the specimen that has been brought into normally consolidated states.

These aspects can be seen more clearly from Fig. 6. Here the effective pressure, p', at the base of the specimen is plotted against the elapsed time on a logarithmic scale. The preconsolidation pressure, p_c', is also indicated on the diagram. It is noted that each of the $p' - \log t$ curves for tests 3, 4 and 5 has an inflection point (or plateau) when the effective pressure, p', at the base of the specimen has just increased to a level sensibly above p_c'. This is a consequence of the strain-rate dependency of yielding pressure (Leroueil et al., 1983; Sekiguchi, 1985) and will be discussed on a quantitative basis in Part II of the present paper.

Figs. 7 and 8 summarize the stress-compressibility data from the present series of isotropic consolidation tests, together with those from the multi-step isotropic consolidation tests separately conducted. The consolidation period in the latter series of tests was chosen to be 1 day for the consolidation pressures $p \leqq 25$ kgf/cm² (2.45 MPa), while the consolidation period under the consolidation pressures $p >$ 25 kgf/cm² (2.45 MPa) was chosen in the range of 9900–14400 minutes. Let us discuss Fig. 7 first. The open circles on this figure correspond to the final readings of the present isotropic consolidation tests. The swelling process following the consolidation phase in test 5 is also indicated for reference. The results of the separate series of multi-step isotropic

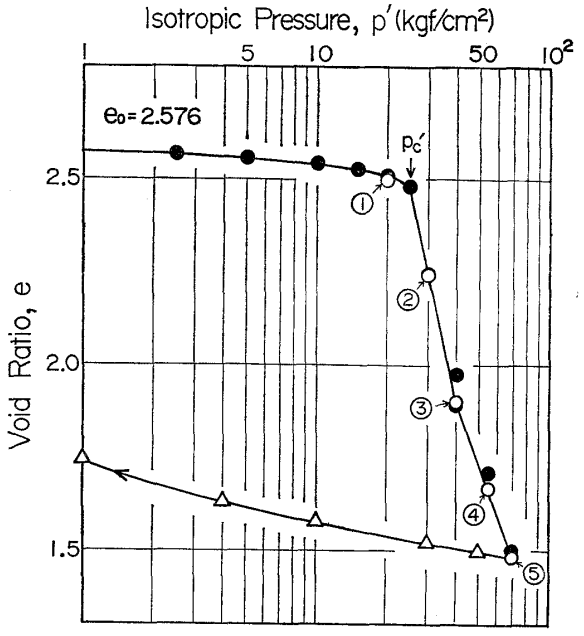

Fig. 7. Measured stress-compressibility performance in e — log p' diagram

consolidation tests are plotted with the solid circles. They clearly show that the specimens underwent a rapid increase in compressibility when a critical pressure equal to 25 kgf/cm^2 (2.45 MPa) was exceeded. Note that this particular value has already been referred to in this paper as the pre-consolidation pressure, p_c', of the mudstone under investigation.

Let λ be the (inelastic) compression index defined by

$$\lambda = -de/d\ln p' = -0.434\, de/d\log p'.$$

Then a closer examination of the compression curve joining the solid circles on Fig. 7 reveals that the compression index is highest in value somewhere around $p'=30$ kgf/cm^2 (2.94 MPa), and then decreases gradually with increasing pressure. The largest value of the compression index is: $\lambda=1.234$. Such a pressure dependency of the compression index will receive a proper allowance in the analyses described in part II of the present paper.

Let us now discuss Fig. 8. Only the compressibility of the specimens before initial yielding is depicted in this figure, on the basis of test 1 in the present series (marked by the open circle) and of the tests separately performed (marked by the solid circles). The data points proved to be best fitted with a straight line through the origin as indicated, giving $K=1043$ kgf/cm^2 (102.2 MPa). Here K is the bulk modulus in terms of effective stress and will be referred to again later.

Let α be the secondary compression index, which is defined as

$$\alpha = d\varepsilon_v/d\ln t = 0.434\, d\varepsilon_v/d\log t.$$

Fig. 9 shows the relations between the secondary compression index and consolidation pressure in the present series of five isotropic consolidation tests. The following points can be made. First, the tendency of secondary compression of the mudstone before initial yielding is weak, if any. Second, the mudstone exhibits secondary compression at the highest rate in terms of α when loaded sensibly beyond the pre-consolidation pressure. Third, its rate of secondary compression in terms of α decreases remarkably with increasing pressure and comes to a practically constant level at high pressures. It is of interest to mention that basically

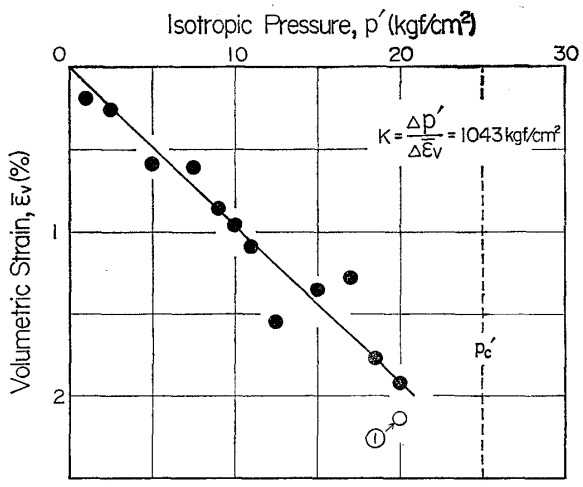

Fig. 8. Measured stress-compressibility performance within a domain of overconsolidation

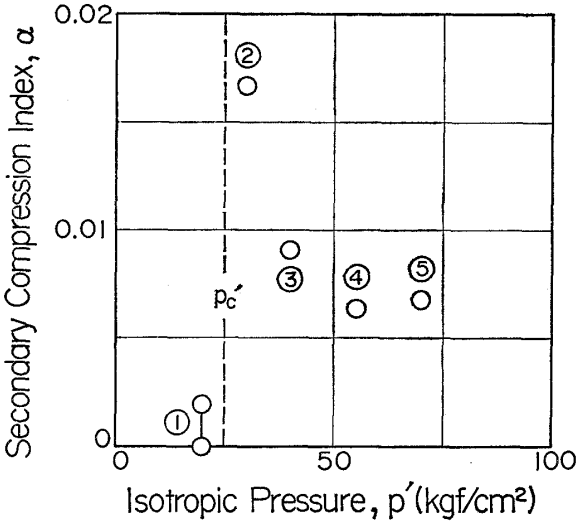

Fig. 9. Measured variation in the coefficient of secondary compression with consolidation pressure

the same features have been observed for naturally cemented clays (Walker and Raymond, 1968; Mesri and Godlewski, 1977).

Falling-Head Permeability Tests

The results of the permeability tests are indicated in Fig. 10, in the form of e versus $\log k$. Here k stands for the coefficient of permeability, and e represents the void ratio in each of the permeability tests. It is seen that the data points can be fitted with a straight line taking the following form:

$$e = e_o + C_k \log (k/k_o)$$
$$= e_o + \lambda_k \ln (k/k_o).$$

Here k_o is a reference value of k at $e = e_o$,

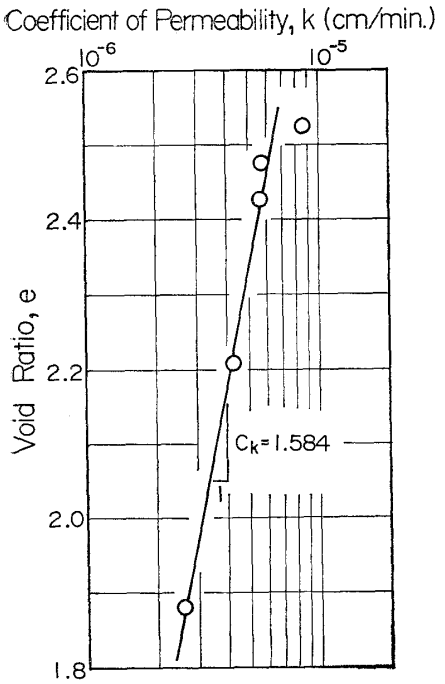

Fig. 10. Measured variation in the coefficient of permeability with void ratio

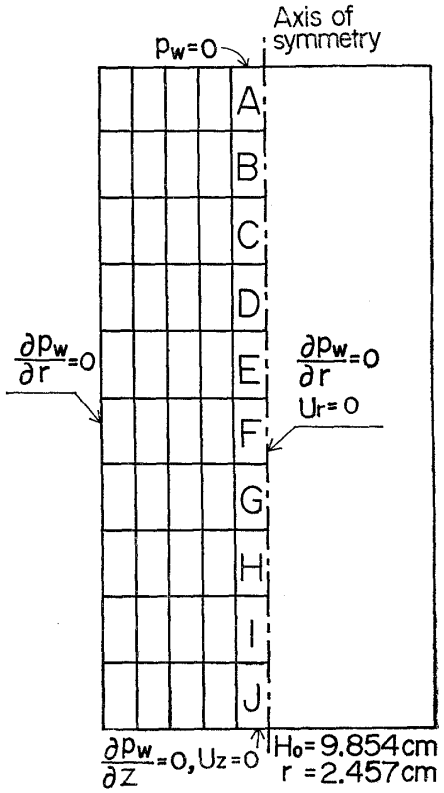

Fig. 11. Finite-element discretization adopted

and $\lambda_k = 0.434\ C_k$ represents a material constant governing the rate of change in permeability due to the change in void ratio. The value of $\lambda_k = 0.688$ thus determined will be used in the consolidation analyses described later.

PART II
ELASTO-VISCOPLASTIC CONSOLIDATION ANALYSES

METHOD OF ANALYSIS

Coupled stress-flow analyses using the method of finite elements were performed to lead to an integrated understanding of the performance of the isotropic consolidation tests described in part I. The results of analyses will be presented in the subsequent sections.

The finite-element code used in the present study is basically the same as that developed by Sekiguchi, Nishida and Kanai (1981). Fig. 11 shows the finite-element mesh adopted for the present analyses, together with the boundary conditions imposed. Only the half of the triaxial specimen is discretized as indicated, in view of the axi-symmetric nature of the problem. Four-noded, isoparametric ring elements are used. The primary unknowns associated with a single element consist of two displacement-increments at every node, together with an excess porewater pressure at the element centroid. The equations of equilibrium and continuity are formulated in terms of such unknowns, along with elasto-viscoplastic constitutive relations for the skeleton and Darcy's law for the porewater flow. The finite-element equations assembled in a matrix form are solved using the method of Gaussian elimination.

ELASTOV-ISCOPLASTIC CONSTITUTIVE MODEL ADOPTED

An elasto-viscoplastic constitutive model developed by Sekiguchi (1977) was implemented into the analysis procedure.

The basic assumption of the model is that the total strain rate, $\dot{\varepsilon}_{ij}$, consists of the viscoplastic and elastic parts as follows:

$$\dot{\varepsilon}_{ij}=\dot{\varepsilon}_{ij}^{p}+\dot{\varepsilon}_{ij}^{e} \quad (1)$$

where the superscripts p and e denote the viscoplastic and the elastic part, respectively.

The viscoplastic strain rate, $\dot{\varepsilon}_{ij}^{p}$, is specified in terms of "static" yield function f as follows:

$$\dot{\varepsilon}_{ij}^{p}=\frac{\partial f/\partial\sigma_{ij}'}{\partial f/\partial p'}\left[\left\{1-\exp\left(-\frac{\varepsilon_v^{p}}{\alpha}\right)\right\}\cdot\frac{\partial f}{\partial\sigma_{kl}}\dot{\sigma}_{kl}'+\dot{v}_o\exp\left(\frac{f-\varepsilon_v^{p}}{\alpha}\right)\right]. \quad (2)$$

Here, σ_{ij}' is the effective stress tensor, ε_v^{p} is the viscoplastic volumetric strain, α is the secondary compression index and $\dot{v}_o$ is the reference volumetric strain rate. In order to keep the present discussion simple, let us introduce the following form of the static yield function:

$$f=\frac{\lambda-\kappa}{1+e_o}\ln(p'/p_c') \quad (3)$$

where λ is the inelastic compression index, defined earlier, κ is the so-called swelling index and p_c' is the pre-consolidation pressure.

The elastic response is assumed to obey

$$\dot{\varepsilon}_{ij}^{e}=\frac{1}{3K}\dot{p}'\delta_{ij}+\frac{1}{2G}\dot{s}_{ij} \quad (4)$$

for $f\leq 0$, and

$$\dot{\varepsilon}_{ij}^{e}=\frac{\kappa}{3(1+e_o)}\frac{\dot{p}'}{p'}\delta_{ij}+\frac{1}{2G}\dot{s}_{ij} \quad (5)$$

for $f>0$. Here K is the bulk modulus, G the modulus of shear rigidity and s_{ij} the deviatoric stress tensor. It is important to note that the swelling index, κ, may be related to the bulk modulus, K, in the form:

$$\kappa=\frac{p_c'(1+e_o)}{K} \quad (6)$$

in view of the "continuity of elastic compressibility" at $p'=p_c'$.

Let us derive a specific equation governing the intrinsic creep of the skeleton. Consider that the effective pressure, p', is increased instantaneously from a starting value, p_o', to a final value, $p_f'>p_c'$, and then maintained constant with time. It then follows that

$$\varepsilon_v(t)=\frac{1}{K}(p_c'-p_o')+\frac{\kappa}{1+e_o}\ln(p_f'/p_c')+\alpha\ln\left[1+\frac{\dot{v}_o\cdot t}{\alpha}\exp(f/\alpha)\right] \quad (7)$$

where

$$f=\frac{\lambda-\kappa}{1+e_o}\ln(p_f'/p_c'). \quad (8)$$

Eq. (7) will later be referred to as the intrinsic creep equation. The adjective "intrinsic" is used to emphasize that Eq. (7) deals solely with the volumetric creep which is intrinsic to the soil skeleton (Sekiguchi et al., 1985). Thus no hydrodynamic time lag is involved in Eq. (7) itself. The third term on the right-hand side of Eq. (7), *i.e.* the viscoplastic component of volumetric strain ε_v^{p}, is zero at $t=0$ as a consequence of the formulation.

DETERMINATION OF CONSTITUTIVE PARAMETERS

The constitutive parameters were determined on the basis of the experimental results described in part I, and are summarized in Table 2.

A remark first made is as to how the pressure-dependency of the compression index (Fig. 7) is allowed for in the present analyses. A sort of a secant modulus on the $e-\log p'$

Table 2 Consititutive parameters determined

	Pressure condition (kgf/cm²)			
	0.5→30	0.5→40	0.5→55	0.5→70
Compression index: λ	1.234	1.234	1.031	0.957
Secondary compression index: α	0.0167	0.0091	0.0066	0.0066

Common values

Initial void ratio: $e_o=2.573$

Pre-consolidation pressure: $p_c'=25$ kgf/cm² (2.45 MPa)

Bulk modulus: $K=1043$ kgf/cm² (102.2 MPa)

Swelling index: $\kappa=0.0857$

Reference volumetric strain rate: $\dot{v}_o=0.22\times10^{-5}$/minute

Initial coefficient of permeability: $k_o=0.71\times10^{-5}$ cm/minute

Rate of permeability change due to the void ratio: $\lambda_k=0.688$

diagram is actually adopted as the compression index, depending on the value of p_f'. That is to say, use is made of the slope of a segment that connects the point of initial yielding to the point of final readings for each consolidation test. The pressure-dependency of the coefficient of secondary compression (Fig. 9) is allowed for in a similar, approximate fashion. That is, the value of α measured in each consolidation test is directly used for the analysis of that particular test.

The procedure of determining the reference volumetric strain rate, $\dot{v}_o$, deserves a remark as well. Recallthat the intrinsic creep equation (7) contains the reference volumetric strain rate as a parameter, and that this particular equation should govern the behaviour of the specimen after the excess porewater pressures have substantially dissipated. These features permit the reference volumetric strain rate to be backfigured on the basis of the observed volumetric behaviour. Specifically, the overall volumetric strain at an arbitrarily chosen time of t=2880 minutes under given stress conditions was used in Eq. (7) to give a value of $\dot{v}_o$ for that particular test. Such calculations for tests 2, 3, 4 and 5 showed that the reference volumetric strain rate falls in the range between 0.133×10^{-5} min^{-1} and 0.308×10^{-5} min^{-1}. It was then decided to take the average value of 0.22×10^{-5} min^{-1} as the representative of the reference volumetric strain rate. No such calculation was needed for test 1, because the entirely elastic response was assumed in the consolidation analysis.

The procedure of determining the other parameters was straightforward, and their values are summarized in Table 2.

COMPARISON BETWEEN THE CALCULATED AND MEASURED PERFORMANCES

Figs. 12(a) through (e) show the calculated and measured volumetric behaviour in all the five isotropic consolidation tests. The corresponding performances of the dissipation of excess porewater pressures at the base of the specimen, are shown in Figs. 13 (a) through (e).

In the present analysis no creep is assumed to occur before the initial yielding. Thus the calculated curve in Fig. 12 (a) exhibits a tendency to converge to a horizontal line after an elapsed time of 30 minutes has been exceeded, whereas the experimental curve indicates a marginal creep there.

The significance of creep deformation may be well conceived from test 2 (see Fig. 12(b)). The broken curve is based on Eq.(7) and represents the intrinsic creep behaviour of the skeleton at constant effective stress. The solid curve represents the calculated, overall volumetric behaviour of the specimen. Thus the delay in the development of overall volumetric strains in the early phase should be regarded as a consequence of the "partial drainage", the very nature of consolidation. Indeed, the solid curve tends to merge into the intrinsic creep curve as time elapses. Essentially the same predicted pattern of behaviour can be

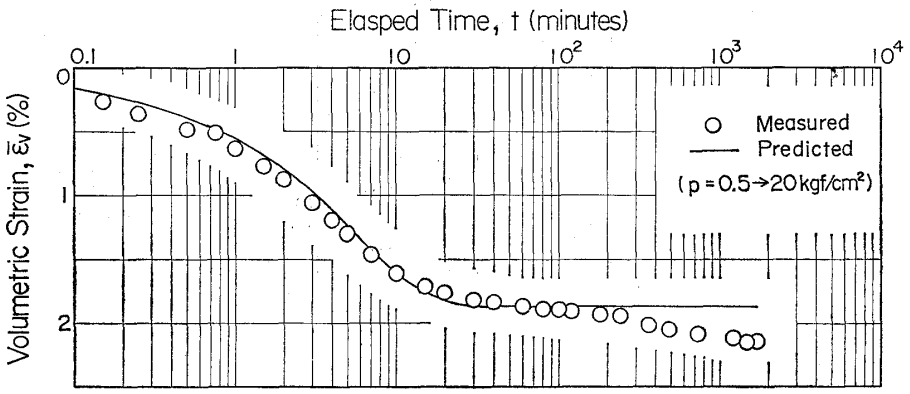

(a)

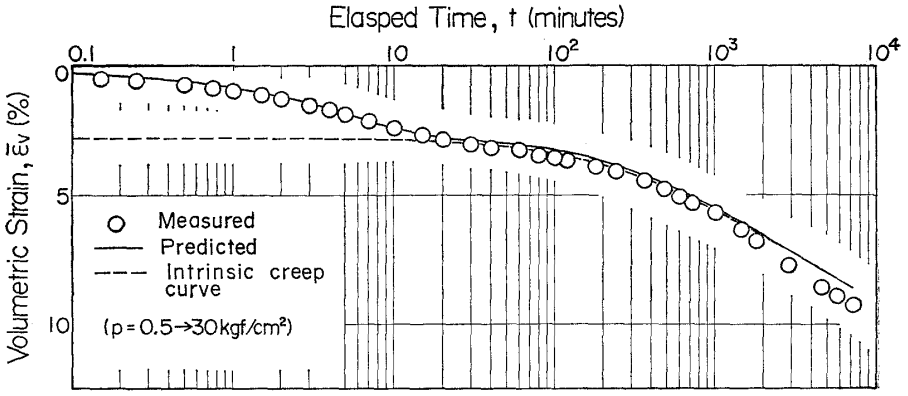

(b)

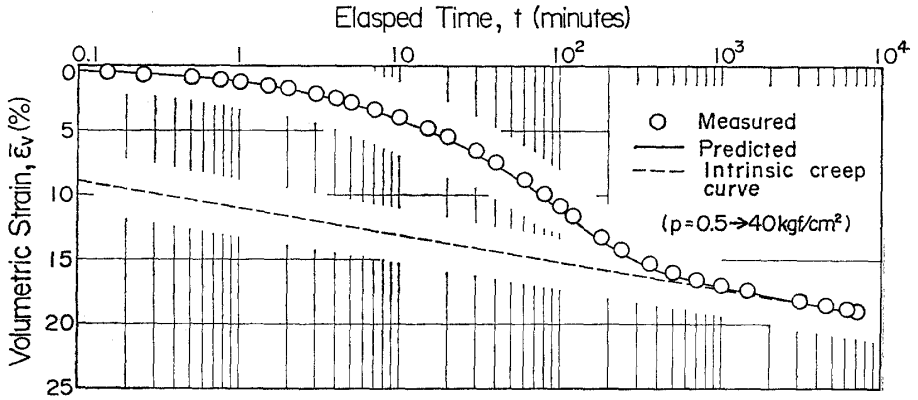

(c)

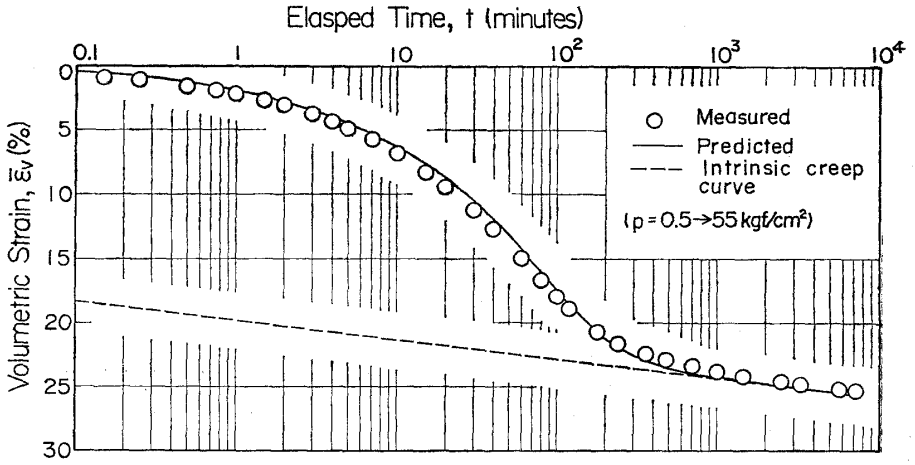

(d)

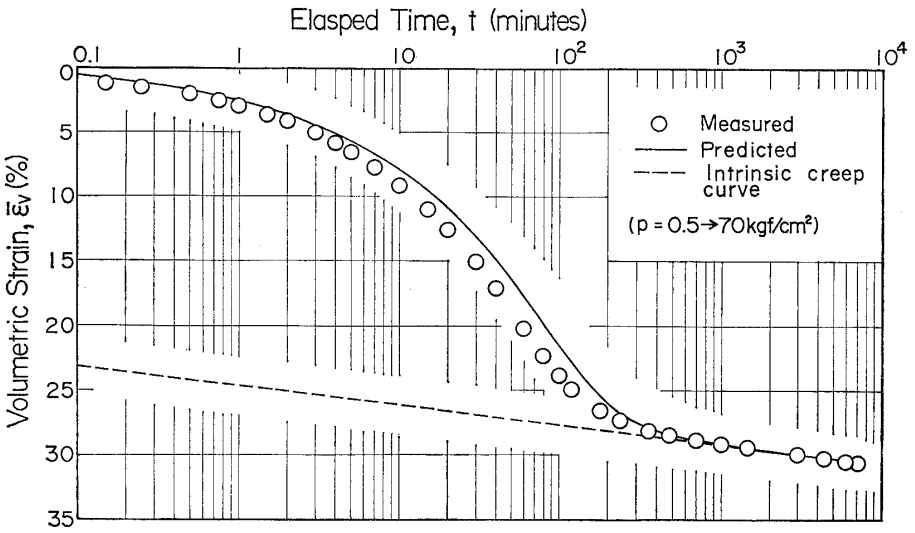

(e)

Fig. 12. Calculated and measured performances of compression with time

(a) p=0.5～20kgf/cm² (b) p=0.5～30kgf/cm²
(c) p=0.5～40kgf/cm² (d) p=0.5～55kgf/cm²
(e) p=0.5～70kgf/cm²

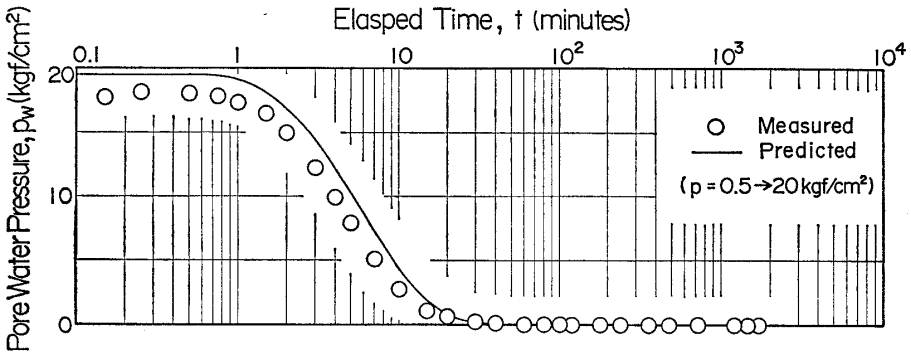

(a)

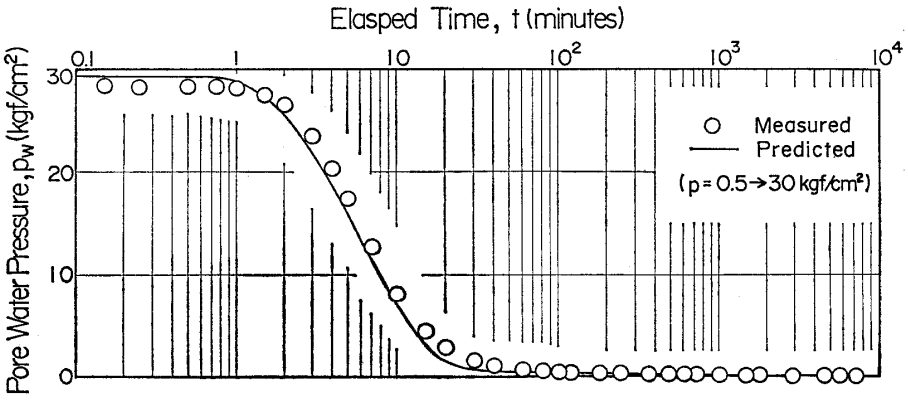

(b)

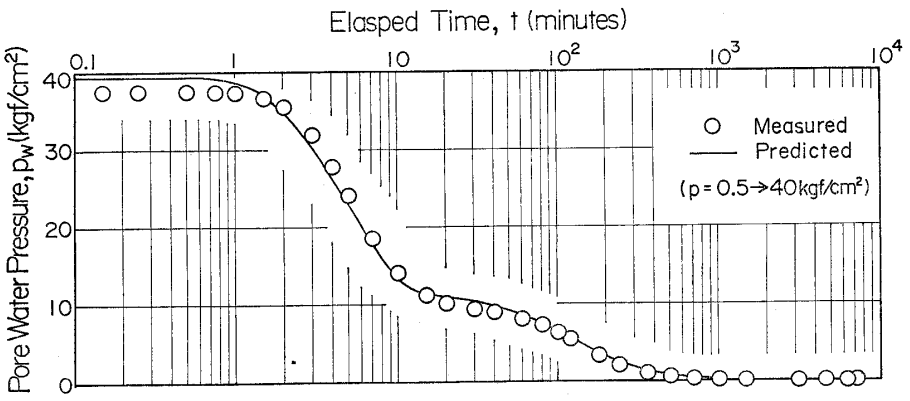

(c)

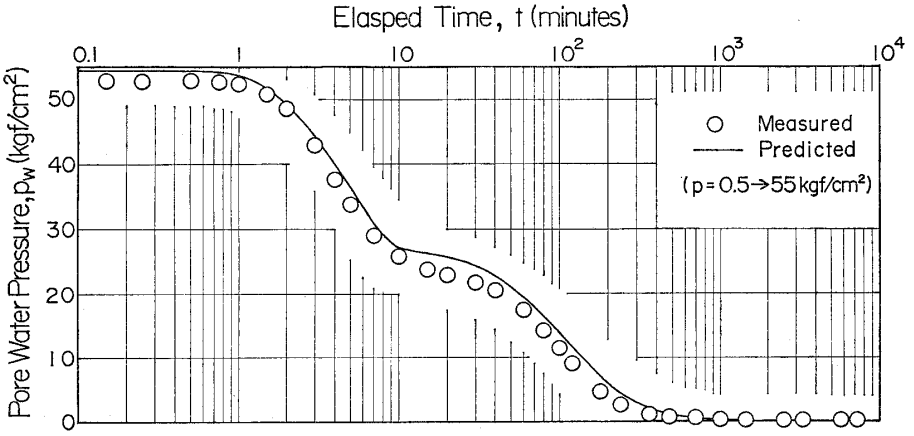

(d)

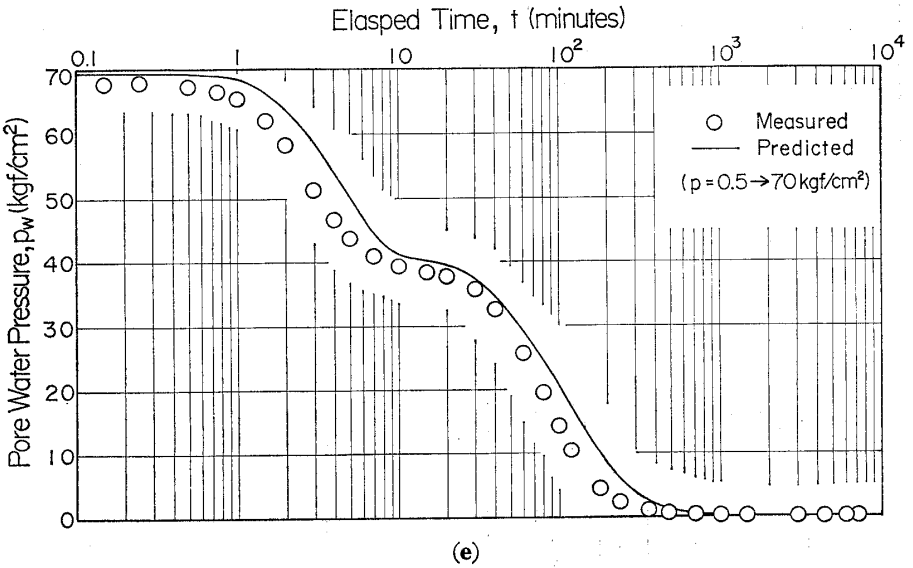

(e)

Fig. 13. Calculated and measured performances of dissipation of excess porewater pressures with time

(a) $p=0.5\sim20$ kgf/cm² (b) $p=0.5\sim30$ kgf/cm²
(c) $p=0.5\sim40$ kgf/cm² (d) $p=0.5\sim55$ kgf/cm²
(e) $p=0.5\sim70$ kgf/cm²

seen for tests 3, 4 and 5, with the influence of partial drainage getting higher (Figs. 12 (c), (d), (e)). It should be noted that the calculated performances of overall volumetric behaviour compare favourably with the corresponding measured performances.

Good agreement between the calculated and measured performances of dissipation of excess porewater pressures can be noted from Figs. 13. The $p_w - \log t$ curves of double sigmoid are nicely reproduced for tests 3, 4, and 5, as shown in Figs. 13(c), (d), (e). Such a double sigmoidal pattern is characteristic of the consolidation behaviour of a specimen when it turns itself from overconsolidated to normally consolidated, while the total stress is maintained constant for $t > 0$. Note that this interesting behaviour also is beyond the scope of classic theories of consolidation.

DISCUSSION

The predictive capability of the elasto-viscoplastic model has proved to be reasonably good. It should, however, be admitted that the measurements were limited to the overall

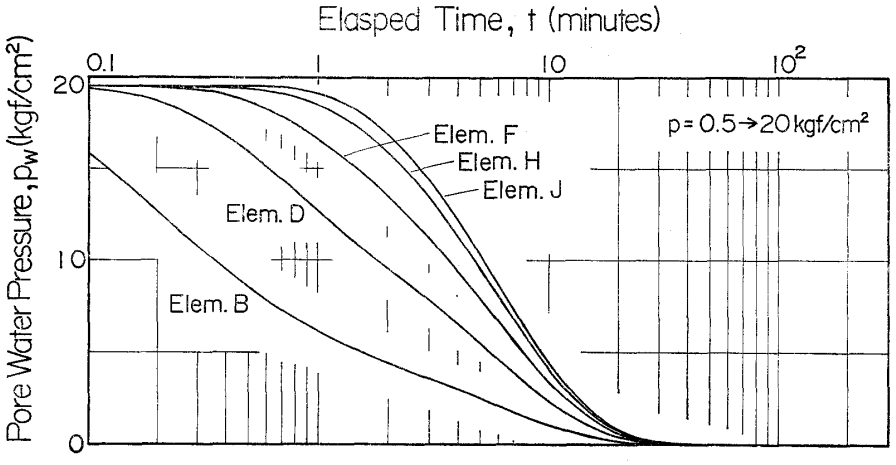

(a)

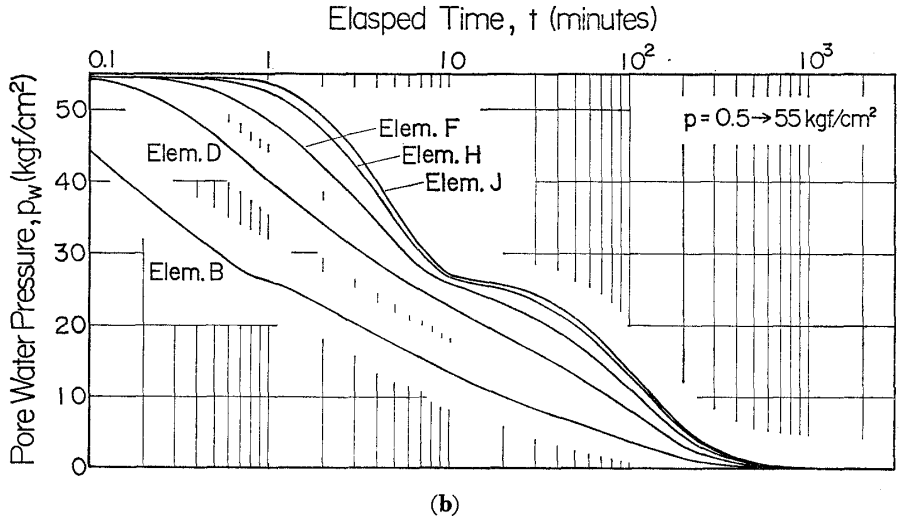

(b)

Fig. 14 Calculated performances of the dissipation of excess porewater pressures at five elements
(a) the behaviour when remaining overconsolidated
(b) the behaviour when undergoing initial yielding

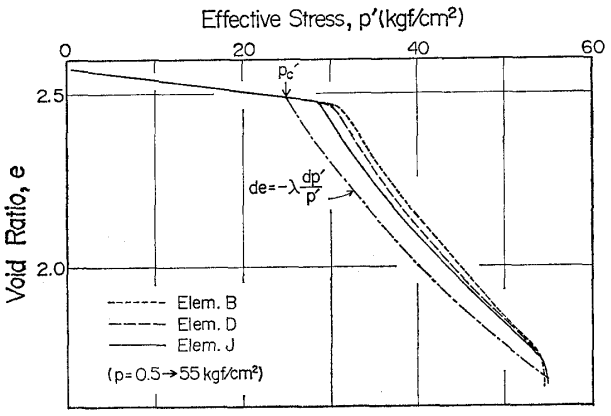

Fig. 15. Calculated state paths of three individual elements in a specimen undergoing consolidation

volume-changes of the specimen as well as the excess porewater pressures at the base of the specimen. More detailed discussion will be possible if the information on the behaviour of individual elements of a specimen undergoing consolidation becomes available. Such attempts have been made for clays by several investigators (Berre and Iverson, 1972; Aboshi et al., 1981; Mesri and Choi, 1985 among others). It was thus decided to present subsequently some additional results of calculation so as to encourage the future research in that direction.

Fig. 14 typifies the predicted differences in the rate of dissipation of the excess porewater pressures in five different elements of a specimen. The locations of those elements are indicated in Fig. 11. The behaviour when the specimen remains elastic is illustrated in Fig. 14(a) for a reference of comparison. The behaviour when the specimen undergoes initial yielding during consolidation, is exemplified in Fig. 14(b). It is interesting to note that the double sigmoidal pattern is manifested by such elements as J, H and F, which are located nearer to the impermeable base of the specimen.

Fig. 15 exemplifies the state paths that are followed by three representative elements B, D and J in a specimen undergoing consolidation. The locations of those elements in the specimen are indicated in Fig. 11. A closer look at the state paths of elements J, D and B on Fig. 15 reveals that the yield pressure of an individual element tends to increase as the element is located nearer to the drainage boundary and is subjected to higher strain rates. Indeed, such a rate-dependency of yield pressure is a consequence of the elasto-viscoplastic formulation adopted in the present study. Let us now look at the chain-dotted line on Fig. 15. This represents the inviscid, elastoplastic response that would be exhibited by all the elements in the specimen if the intrinsic rate-dependency of the skeleton was totally absent. Note that the experimental evidence in this study has consistently favoured the elasto-viscoplastic formulation. This does not assert that the compressibility of diatomaceous mudstones is completely understood. Rather, it is felt that the compressibility modelling at and around the pre-consolidation pressure needs a scrutiny.

It is hoped that the foregoing discussions arouse a further interest in the compressibility of naturally cemented diatomaceous mudstones, in close relation to the behaviour of naturally cemented Pleistocene clays as well as alluvial clays treated by means of cementing agents.

CONCLUSIONS

The isotropic consolidation behaviour of a diatomaceous mudstone from Suzu, Noto Peninsula has been discussed in detail. The mudstone may be best featured as a naturally emented material with a highly porous skeleton. Part I of the paper has indicated: (1) the compressibility of the mudstone increases rapidly when loaded beyond the pre-consolidation pressure; (2) the secondary compression is negligibly small before the initial yielding, but becomes very significant when loaded sensibly above the pre-consolidation pressure; and (3) the logarithm of the coefficient of permeability decreases linearly withdecreasing void ratio. The basic, experimental aspects of elasto-viscoplastic consolidation have been summarized in Part I of the paper, and their detailed analyses have been performed in Part II. A series of coupled stress-flow analyses has been made using the method of finite elements, along with an adapted version of the

elasto-viscoplastic constitutive model(Sekiguchi, 1977). It has been shown that the predicted performances of consolidation compare favourably with the measured performances, thus validating the usefulness of the constitutive model adopted.

ACKNOWLEDGMENTS

The authors were deeply indebted to Dr. T. Matsumoto at the Kanazawa University for considerable assistance with the computer analysis. The finite element computations were performed at the Computer Center of the Kanazawa Institute of Technology.

REFERENCES

1) Aboshi, H., Matsuda, H. and Okuda, H. (1981): "Preconsolidation by separate-type consolidometer," Proc. 10th Int. Conf. Soil Mech. Found. Eng., Stockholm, Vol. 3, pp. 577-580.
2) Berre, T. and Iversen, K. (1972): "Oedometer tests with different specimen heights on a clay exhibiting large secondary compression," Géotechnique, Vol. 22, pp. 53-70.
3) Leonards, G. A. and Girault, P. (1961): "A study of the one-dimensional consolidation test," Proc. 5th Int. Conf. Soil Mech. Found. Eng., Paris, Vol. 1, pp. 213-218.
4) Leroueil, S., Tavenas, F., Samson, L. and Morin, P. (1983): "Preconsolidation pressure of Champlain clays. Part II. Laboratory determination," Canadian Geotech. Journal, Vol. 20, pp. 803-816.
5) Maekawa, H. and Miyakita, K. (1983): "Mechanical properties of diatomaceous soft rock," Proc. Japan Soc. Civil Engrs, No. 334, pp. 135-143 (in Japanese).
6) Mesri, G. and Choi, Y. K. (1985): "The uniqueness ofthe end-of primary (EOP) void ratio-effective stress relationship," Proc. 11th Int. Conf. Soil Mech. Found. Eng., San Francisco, Vol. 2, pp. 587-590.
7) Mesri, G. and Godlewski, P. M. (1977): "Time- and stress- compressibility interrelationship," J. Geotech. Eng. Div., ASCE, Vol. 103, No. GT 5, pp. 417-430.
8) Nishida, Y., Sekiguchi, H., Matsumoto, T., Hosokawa, S. and Hirose, T.(1985): "Drivability of steel pipe piles into diatomaceous mudstone in the construction of Notojima bridge," Proc. Int. Symp. on Penetrability and Drivability of Piles, San Francisco, Vol. 1, pp. 187-190.
9) Sekiguchi, H. (1977): "Rheological characteristics of clays," Proc. 9th Int. Conf. Soil Mech. Found. Eng., Tokyo, Vol. 1, pp. 289-292.
10) Sekiguchi, H. (1985): "Macrometric approaches -Static- Intrinsically time-dependent," Report of ISSMFE Subcommittee on Constitutive Laws of Soils, San Francisco, pp. 66-98.
11) Sekiguchi, H., Nishida, Y. and Kanai, F. (1981): "Analysis of partially-drained triaxial testing of clay," Soils and Foundations, Vol. 21, No. 3, pp. 53-66.
12) Sekiguchi, H., Nishida, Y., Matsumoto, T. and Uesawa, M. (1985): "Characterization of a diatomaceous mudstone by elasto-viscoplasticity," Proc. 5th Int. Conf. Numerical Methods in Geomechanics, Nagoya, pp. 437-444.
13) Walker, L. K. and Raymond, G. P. (1968):"The prediction consolidation rates in a cemented clay," Canadian Geotech. Journal, Vol. 5, No. 4, pp. 192-216.
14) Yamada, T. and Matsuse, K. (1981): "Plan and design of the Notojima bridge," KYORYO-TO-KISO, No. 3, pp. 32-39 (in Japanese).